Journal of Physics:
Conference Series

PAPER • **OPEN ACCESS**

A MATLAB/Simulink model of a parallel hybrid PEMFC/battery powertrain for passenger cars

To cite this article: D. Parmiggiani *et al* 2024 *J. Phys.: Conf. Ser.* **2893** 012070

Journal of Physics: Conference Series **2893** (2024) 012070 doi:10.1088/1742-6596/2893/1/012070

A MATLAB/Simulink model of a parallel hybrid PEMFC/battery powertrain for passenger cars

Parmiggiani D.[1*], Antetomaso C.[2], Martoccia L.[1], Merola S.[3], d'Adamo A.[1]

[1] Department of Engineering "Enzo Ferrari", University of Modena e Reggio Emilia, Via Vivarelli, 10, 41125, Modena, Italy
[2] University of Naples "Parthenope", Via Amm. Acton, 38, 80133 Napoli Italy
[3] CNR-STEMS, Via Guglielmo Marconi, 4, 80125, Naples, Italy

[*]246128@studenti.unimore.it

Abstract. The transition towards sustainable transportation solutions needs the development of efficient and environmentally friendly propulsion systems. Among these, Proton Exchange Membrane Fuel Cells (PEMFCs) seem to be a promising solution for sustainable powertrain design. This study presents the development of a MATLAB/Simulink model for a parallel hybrid FC/battery system representative of a passenger car, including all the auxiliary components and sub-systems. The model incorporates electrochemical, heat transfer, and fluid dynamic processes to accurately simulate the dynamic PEMFC stack and system behaviour. By implementing user-defined initial and boundary conditions, the model offers flexibility in simulating real-world scenarios, allowing the investigation of system performance under different environmental and dynamic driving conditions, as prescribed by the latest homologation protocols. Additionally, it accounts for the membrane degradation, which is a critical aspect affecting long-term durability, performance, and efficiency. Furthermore, a Graphic User Interface (GUI) has been developed to simplify the input of the main parameters, embedding the model in a user-friendly yet comprehensive tool designed for students, researchers, and engineers to evaluate the realizability of these efficient technologies. The intrinsic adaptability to model any FC/battery power system under a generic time-varying load constitutes an additional valuable point of the presented study to enable engineering progress, advancing the energy transition via sustainable powertrain solutions.

1. Introduction

Fuel cell powertrains play a crucial role in the energy transition by offering a sustainable and efficient alternative to traditional combustion engines, significantly reducing greenhouse gas emissions. This hybrid system effectively splits the power demand between the PEMFC stack and the battery, ensuring optimal performance and efficiency under various driving conditions. However, the complexity of a parallel hybrid Fuel Cell/Battery powertrain requires the development of dedicated models to simulate the dynamic behaviour of vehicles, which is the aim of this study.

The developed model presented in this paper incorporates run-time monitors, allowing users to observe critical parameters such as hydrogen (H_2) consumption, stack and system efficiency,

the distribution of power demand between the power sources, battery and electric motor operating points, and the charge/discharge rates (C-rates) of the battery. Users have the flexibility to select the desired drive cycle through a dedicated Graphic User Interface (GUI), including the Worldwide Harmonized Light Vehicles Test Procedure (WLTP), New European Driving Cycle (NEDC), Worldwide Motorcycle Test Cycle (WMTC), Supplemental Federal Test Procedure (SFUDS), constant velocity driving, as well as generic drive cycles. The model allows the simulation of user-defined conditions on a roller bench, where dynamic contributions are taken into account. For the sake of simplicity, the road angle is neglected in this study and it will be implemented in future versions. The model dynamically adjusts the power output of the fuel cell stack and the battery, following a ruled-based strategy. The idea behind this is to define a power split logic based on vehicle power requirement: in low power scenario the ESS is the main energy source while the FC supports energy in case of high power request and to restore the SOC. By these conditions, we ensure a proper use of FC in order to reduce stack components' degradation due to rapid power variations. In addition, we consider the regenerative braking to increase the efficiency and recharge the battery. The EMS is implemented using the State flow tool, which allows to define state machines and flow charts through a useful visual approach. In this work, we use the WLTP for a medium passenger car (Class 3b) and, in order to perform a long-term performance analysis, the initial SOC is restored at the end of the cycle. In fact, this condition is widely respected in the literature ([1], [2], [3], [4]).

2. Numerical model

The Balance of Plant (BoP) will not be presented in this work, as it inherits the model implemented in [5] for a steady-state FC-only system, which is schematically illustrated in Figure 2. In this study the relevant addition of the dynamic operation mode and of the system hybridization with a battery system are presented. With this update the system responds dynamically to a user-defined power demand, even if the efficiencies of the auxiliary components are considered constant (Figure 3), and a rule-based strategy to control the hybrid powertrain is introduced. It is now feasible to energize the ancillary components through the utilization of the battery, thereby enabling the recovery of energy during periods of deceleration and inactivity.

2.1 Voltage losses and membrane degradation model

The potential of a fuel cell is given by the equilibrium potential, i.e. is the maximum possible voltage the cell can achieve under ideal conditions (E_0). However, in real-world applications, this potential is reduced by three primary types of losses: activation losses (η_{act}), ohmic losses (η_{ohm}), and concentration losses (η_{conc}):

$$\eta_{act} = \frac{R\overline{T_{stack}}}{2F\alpha_a}\log\left(\frac{i}{i_{0,a}}\right) + \frac{R\overline{T_{stack}}}{2F\alpha_c}\log\left(\frac{i}{i_{0,c}}\right) \quad [V] \quad (1)$$

$$\eta_{ohm} = iR \quad [V] \quad (2)$$

$$\eta_{conc} = me^{ni} \quad [V] \quad (3)$$

$$V_{cell} = E_0 - \eta_{act} - \eta_{ohm} - \eta_{conc} \quad [V] \quad (4)$$

Where E_0 is the equilibrium potential of the single cell, R is the universal gas constant, $\overline{T_{stack}}$ is the mean temperature between the inlet and the outlet, F is the Faraday constant, $\alpha_{a/c}$ are the anode/cathode charge transfer coefficients, i is the current density within the cell, R is the internal resistance of the cell, m and n are empirical coefficients use to compute the concentration losses and $i_{0,a/c}$ are the exchange current densities of anode and cathode respectively all of which are shared with multidimensional simulation techniques [6], [7], [8], [9]. The most important specifications that describe the stack are listed in the table below.

Table 1. Features of the stack.

Parameter	Unit	Value
Number of cells	-	330
Number of channels per cell	-	50
Effective area of a cell	m^2	0.0303
Maximum power of the stack	kW	122,28

After defining the polarization curve as a function of the current density, it is immediate to obtain the power curve; these two curves, shown in Figure 1, are then the loci of the possible operating points during the simulated drive cycle:

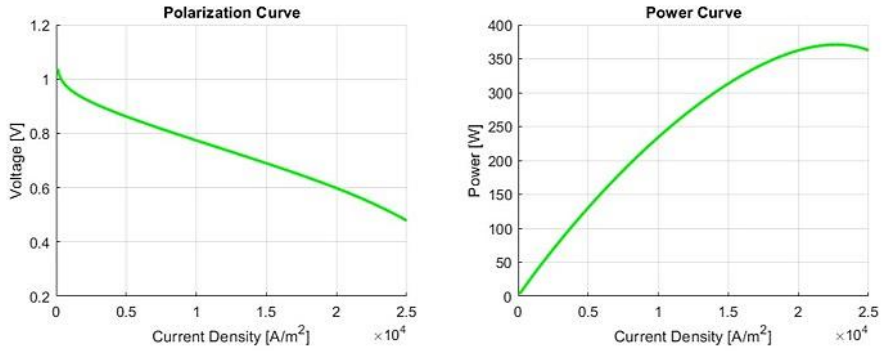

Figure 1. Polarization curve (left) and power curve (right) obtained from the zero-dimensional stack model at the end of the WLTP cycle. Since the user can change the stack configuration, the graph values refer to a single cell.

The selected model for membrane degradation is the analytical model proposed by Karpenko et al. [15], in which the membrane thickness and its ionic conductivity values are updated at each time step. This approach permits a comprehensive and dynamic simulation of the membrane's performance over time, thereby facilitating insights into the impact of degradation on functional properties.

$$\delta_{mem}^{t} = \delta_{mem}^{0}\left(1 - tr_{\delta_{mem}}^{curr}\right) \quad [m] \quad (5)$$

$$\sigma_{mem}^{t} = \sigma_{mem}^{0}\left(1 - tr_{\sigma_{mem}}^{curr}\right) \quad [S/m] \quad (6)$$

In this equation, δ_{mem}^{t} represents the thickness of the membrane, while σ_{mem}^{t} denotes its ionic conductivity. The apex refers to the time step. The degradation rates ($r_{\delta/\sigma_{mem}}^{curr}$) are calculated as a function of the mean temperature of the cell, the relative humidity of the cathode, and cell potential at each iteration.

2.2 Power demand

The power demand of a FCHEV is primarily determined by the power required for the electric motor ($P_{req_{EM}}$), which drives the vehicle, and the additional power needed for various auxiliary components such as air compressor, expander (not linked with the air compressor), intercooler, fan, radiator, humidifier and coolant pump. Together, these components represent the total power demand necessary to follow a given driving cycle. In a parallel hybrid powertrain, this entire power demand is strategically split between two power sources: fuel cell stack (P_{FC}) and battery (P_{bat}).

- $P_{req_{EM}}$ is the required power for the electric motor and is computed through the Vehicle subsystem, which operates as a black box. Input data are resumed in the Table 2:

Table 2. Parameters used to compute the traction force:

Parameter	Unit	Value	Editable
Air density (ρ)	kg/m^3	1.2	In GUI
Frontal area (A_{front})	m^2	2.23	In GUI
Grav. acceleration (g)	m/s^2	9.81	-
Longitudinal acceleration ($dv(t)/dt$)	m/s^2	f(t)	-
Vehicle mass (m)	kg	1920	In GUI
Rolling resistance coefficient (δ)	-	0.01	In GUI
Drag coefficient (C_D)	-	0.29	In GUI
Velocity ($v(t)$)	m/s	f(t)	From '.xlsx'

The vehicle speed is assigned at each timestep by means of a column vector (Structure with Time) stored in an Excel file. Therefore, user must load the file (.xlsx) during the phase of initialization.

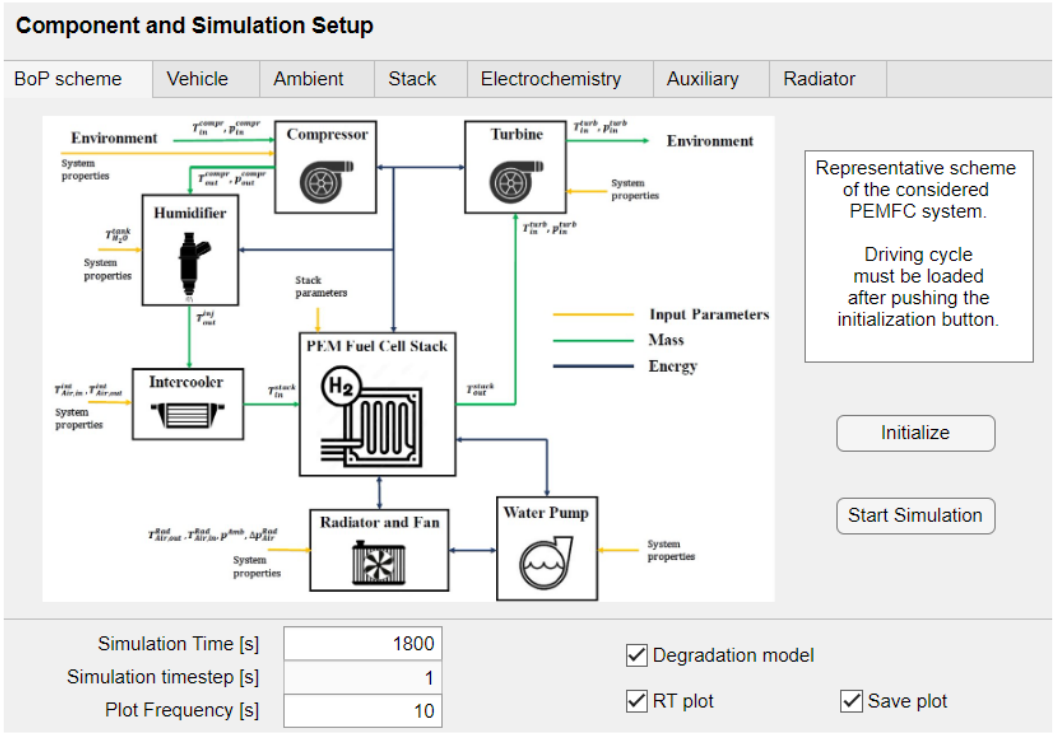

Figure 2. Graphic User Interface (GUI). Only the main interface of the application is displayed here. Users can select the frequency of plotting on the graph, the duration of the simulation, and other graphical characteristics related to the plots.

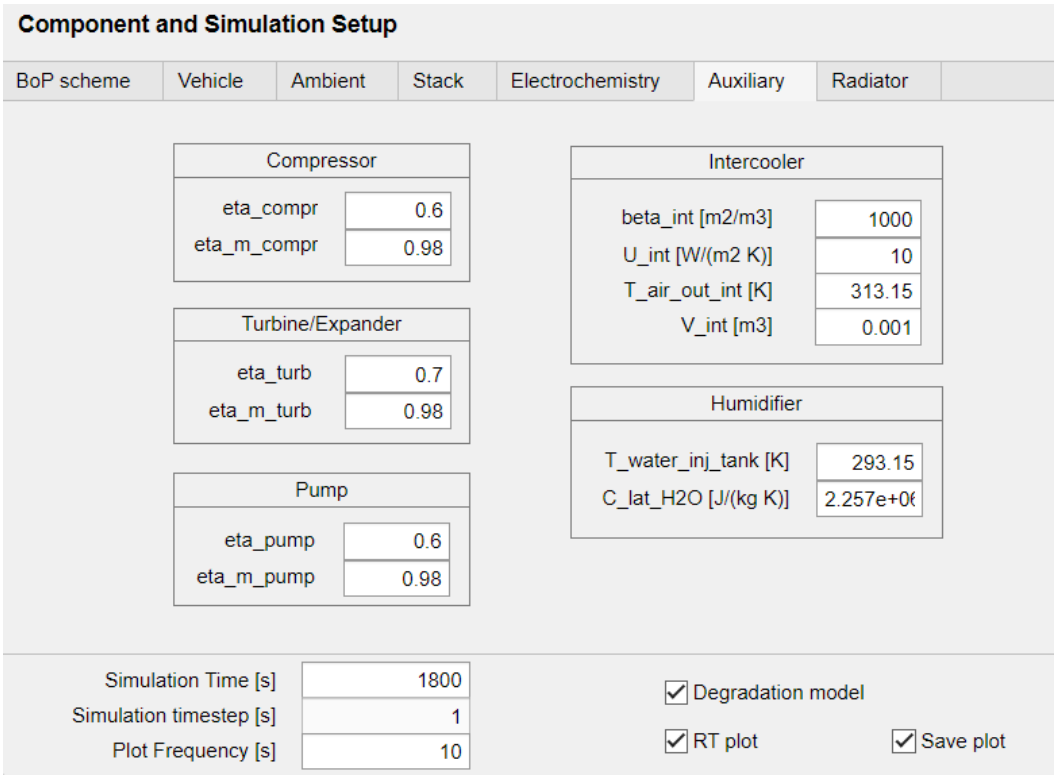

Figure 3. The parameters of the auxiliary components are editable on the interface. It is possible for the user to modify both isentropic and mechanical efficiencies.

Simulation begins by computing the required force for traction F_{tr} :

$$F_{tr} = m\frac{dv(t)}{dt} + \frac{1}{2}C_D v^2(t)\rho A_{front} + mg\delta \quad [N] \quad (7)$$

With the hypothesis of:

$$\frac{dv(0)}{dt} = 0 \quad (8)$$

Since traction force and velocity are known for each timestep, rotational speed and power required from the EM are known too. Obviously, the model accounts for the transmission ratio (τ) and the efficiency (η) of the EM through the map, according to Figure 4.

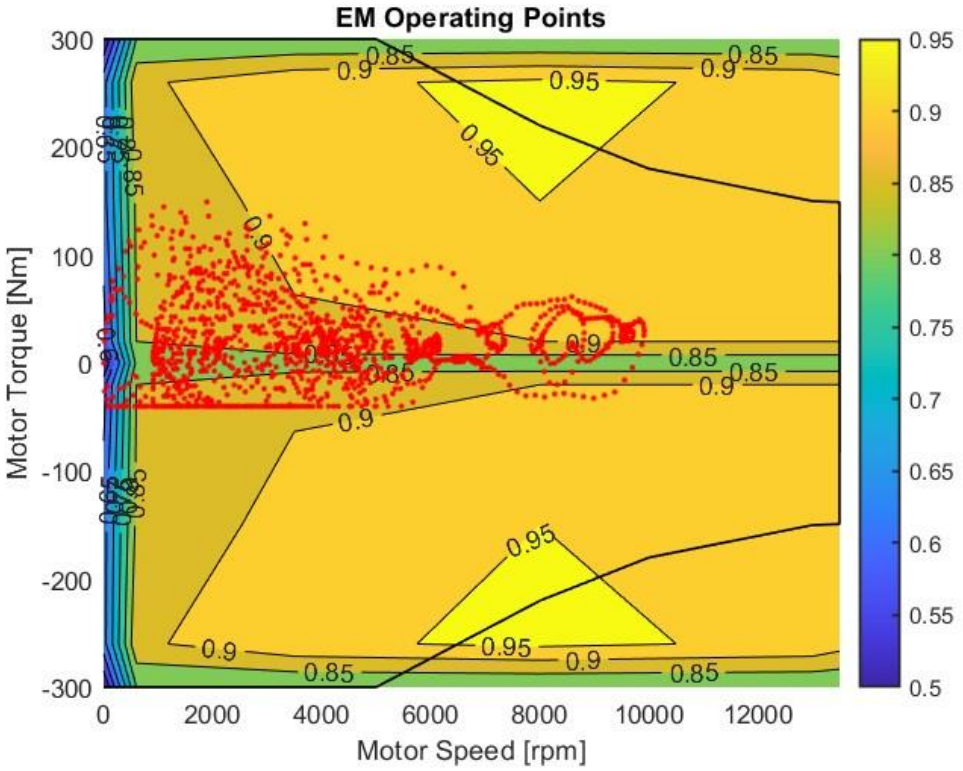

Figure 4. Operating points of the electric motor during a WLTP cycle.

According to [10], to overcome the problem of modelling the inertia of the electric motor, the total mass of the vehicle is increased by 5%.

- P_{FC} and P_{bat} take different values, depending on the strategy, that will be given later.
- P_{aux} is strictly related to P_{FC}, which defines the required hydrogen supply by means of the stack current.

2.3 Battery model

According to the work proposed in [11], [12], the FC stack is coupled with a Nickel-Metal-Hydride (NiMH) battery pack, featuring cells with a capacity of 6.5 Ah (Q_{bat}) connected in series. The logical path and data processed by the model are depicted in the block diagram below. Charging

and discharging resistance are considered equal and constant ($R_{bat,d} = R_{bat,c}$), as well as the temperature and its effect on performance.

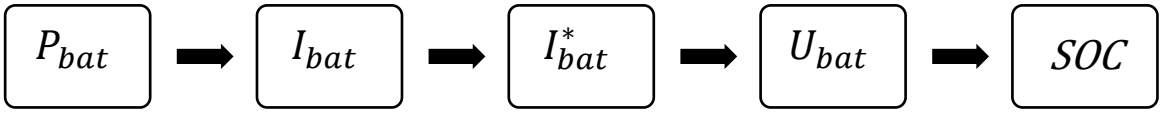

Under the assumption that P_{bat} is negative for charging and positive for discharging, is straightforward to compute the current circulating in the battery I_{bat}:

$$I_{bat} = \frac{U_{bat,oc} - \sqrt{U_{bat,oc}^2 - 4P_{bat}R_{bat}}}{2R_{bat}} \quad [A] \quad (9)$$

$$U_{bat} = U_{bat,oc} - I_{bat}R_{bat} \quad [V] \quad (10)$$

Where $U_{bat,oc}$ is the Open Circuit Voltage (OCV) and I^*_{bat} is the output of a first-order low-pass filter designed for the current. Thus, State of Charge (SOC) is determined by the discrete-time equation:

$$SOC(i) = SOC(i-1) - \frac{I_{bat}\eta_c^{sign(I_{bat})}t}{Q_{bat}} \quad (11)$$

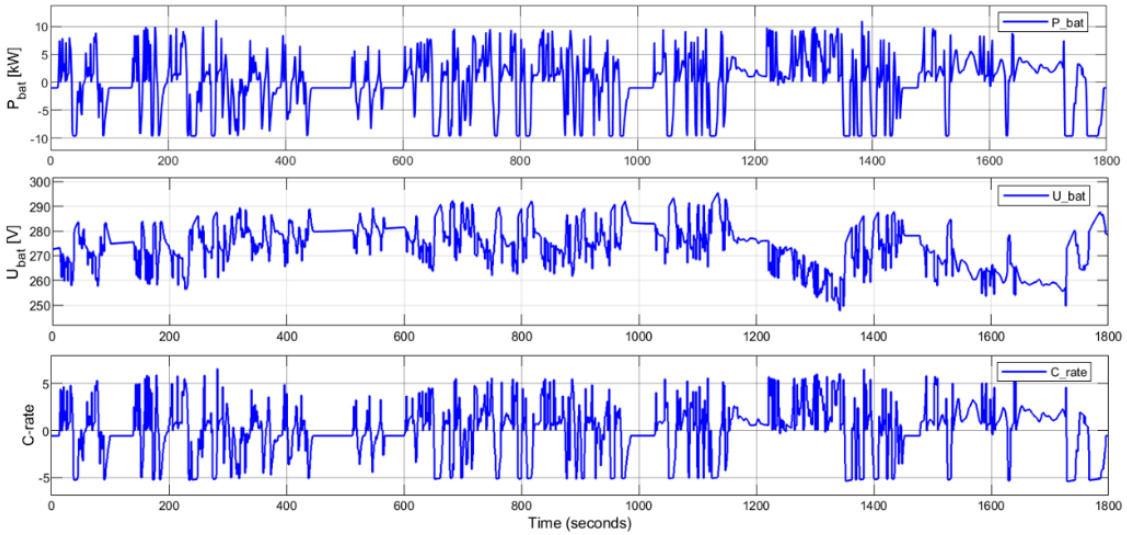

Figure 5. Battery operating parameters during a WLTP cycle.

Here, η_c is the coulomb efficiency and t is the timestep. To assess the operating condition of the battery, the most relevant parameter to observe is the C-rate, which represents the severity of the charging and discharging process. It has been observed that that the C-rate value reaches the maximum value of 6 during the discharging periods of the WLTP cycle, while it's a little lower during charging phase. Figure 5 shows the trend of the main battery parameters while driving a WLTP cycle. The condition often mentioned in the literature ([1], [2], [3], [4]) regarding the maximum power of the battery (20 kW) has been met, since its maximum value during the load cycle is 12 kW.

3. Rule-based strategy

The Energy Management System (EMS) of the powertrain is performed by a rule-based strategy. In fact, the power required by the electric motor defines the operation mode among the four possible choices (idle, battery only, FC only and regenerative braking), while the state of charge quantifies the supply of energy from one source rather than the other one. Simulation starts on idle condition with high SOC and according to these parameters, the system dynamically adjusts the power demand. A brief illustration of the strategy is given in the Figure 6.

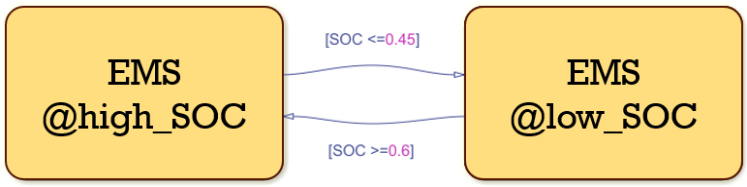

Figure 6. Illustration of the two main operating states, including thresholds.

To ensure that the charging process takes place, the thresholds are non-symmetrical and depend on the current state. For example, if the battery is in the high_SOC state and begins to drain, it will switch to the low_SOC state when the SOC drops below 0.45; then the charging process will begin and will last until the SOC returns above 0.6. Each of the two superstates consists of four operation modes:

$$\begin{cases} Idle\ condition & P_{req_{EM}} = 0 \quad [kW] \\ Battery\ only & 0 < P_{req_{EM}} \leq 6 \quad [kW] \\ FC\ main\ energy\ source & P_{req_{EM}} > 6 \quad [kW] \\ Regenerative\ braking & P_{req_{EM}} < 0 \quad [kW] \end{cases} \tag{12}$$

For the sake of simplicity, only the strategy where the state of charge is greater than 0.6 is reported here, since the other is a linear combination of this one. When the power demand is zero, the stack operates on idle, delivering constant power equal to 500 W and the excess power generated charges the battery; to prevent the cell from shutting down, this limit was also set for the regeneration and battery only phases. Instead, to increase efficiency during the "FC main energy source" phases, the battery helps the stack to reach the required power by providing a fraction (1/3) of the auxiliary power supply. Furthermore, a limit on the maximum regeneratable power has been set. Figure 7 shows stack power output and the battery state of charge during a WLTP cycle.

It is obvious that with these thresholds the state of charge is preserved between the start and end of the simulation. However, thanks to the adaptability of the model, it's possible to simulate the behaviour of different vehicles by modifying the input data through the graphical interface. The aim of this work is not to replicate the behaviour of the Toyota Mirai, but for validation purposes, its hybrid powertrain was chosen as the reference.

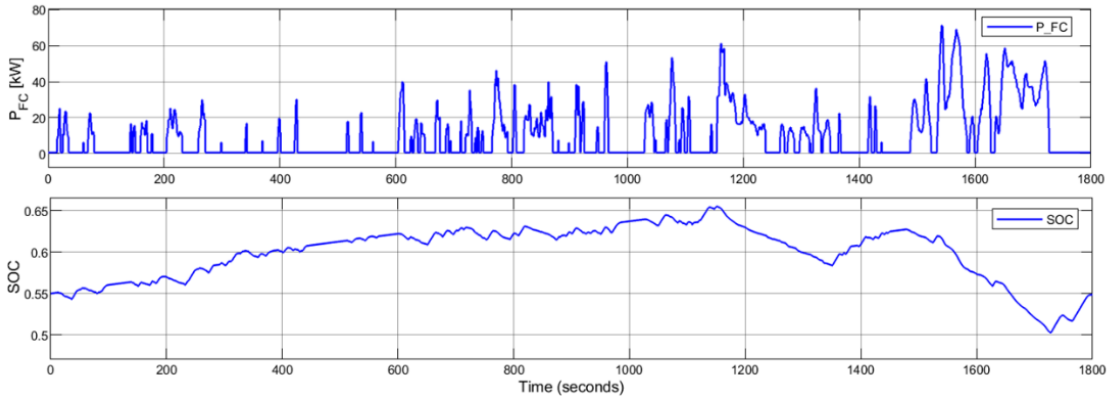

Figure 7. Power output from the stack (top) and state of charge (bottom) during a WLTP cycle.

4. Experimental data and results

Due to their extensive database, experimental data collected by Argonne National Laboratory on the Toyota Mirai model has been used [13], [14]. Using these data, a comparison was made between the strategy proposed in this study and the actual performance. So, the presented EMS is an alternative to the real one and some results will differ from the curves obtained in the laboratory. This approach allowed for a thorough analysis and benchmarking of our methods against a well-established reference. Since our model has a timestep of 1 second while the experimental data are sampled at a frequency of 10 Hz, all data have been adjusted.

There is a high agreement between our simulation and the experimental results regarding the tractive force (F_{tr}). The small differences visible in Figure 8 are due to the unavailability of the actual efficiency maps for the Toyota Mirai electric motor, which necessitated modelling one instead. A comparison was then made between the power delivered by the stack and the corresponding experimental data (Figure 9); in addition, looking at just a few areas of the graph (Figure 10), it can be seen that the EMS used in this study has eliminated the power ripple and helped extend stack life. Another data that can be observed thanks to the zoom is the difference between the real and the implemented idle state, which is set to a higher value.

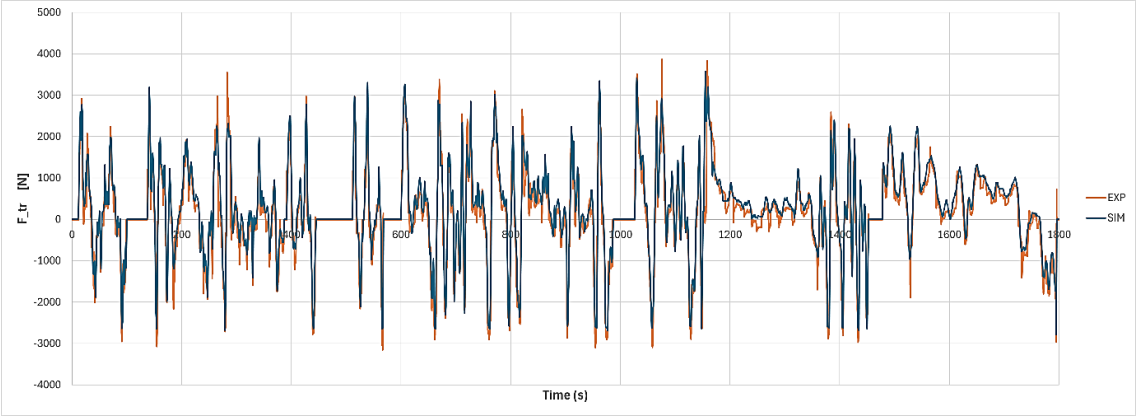

Figure 8. Tractive force required to perform the WLTP cycle.

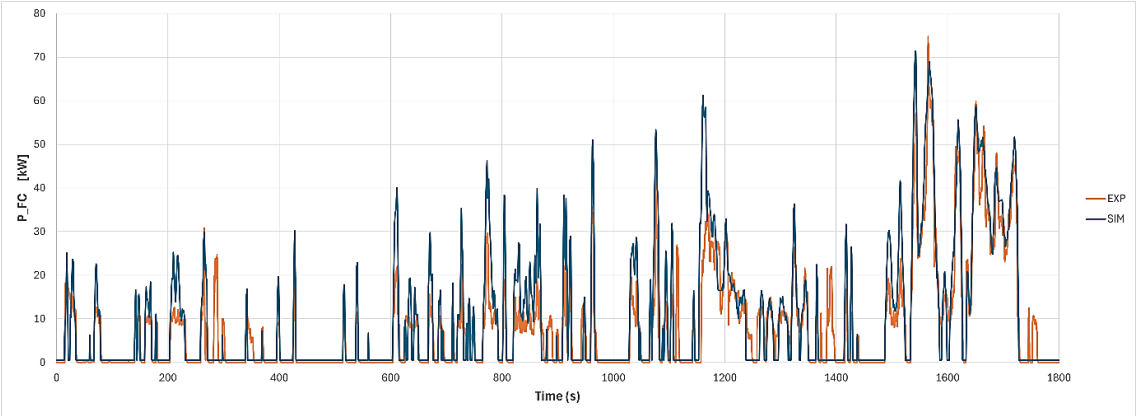

Figure 9. Power required to the stack during a WLTP drive cycle.

Of course, this parameter depends on the strategy, so the result shown should be related to the state of charge of the battery, which is high (SOC > 0.6). For the same reason, the state of charge itself will be different, but it will still be preserved between the beginning and the end of the simulation (Figure 11). It is clear that the battery tends to recharge more than in the real case, which results in a slight increase in hydrogen consumption (Argonne National Laboratory measurements indicate a total consumption of 196.8 grams of hydrogen, while our simulation result is 205.4 grams, Figure 12).

This was chosen because, if stack aging can be monitored using a degradation model proposed by Karpenko et al. [15], it is not possible to do the same for the battery. In fact, this significantly reduces the load on the battery and the power it must handle is lower (Figure 13 and Figure 14); therefore, it delivers lower currents, which greatly increases its lifespan. In the analysis of the battery performance during the simulation and the related experimental data, the difference is noticeable.

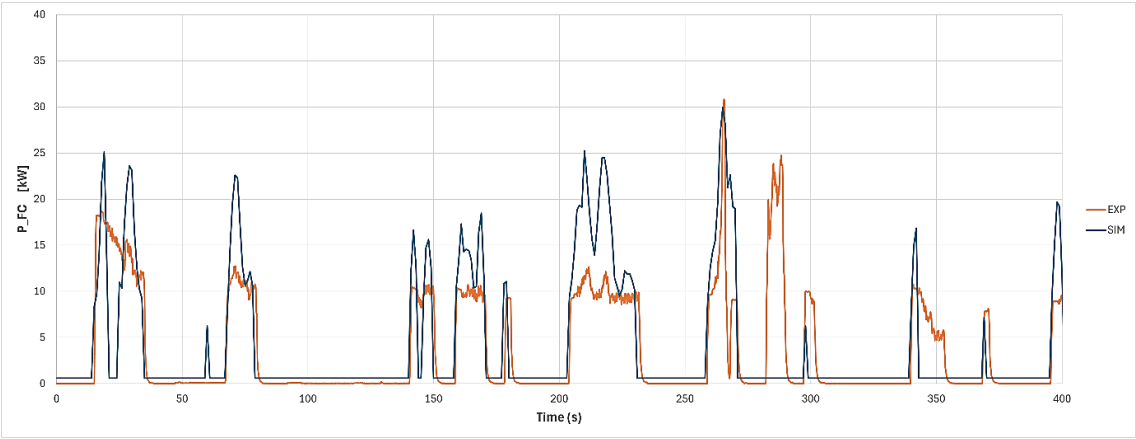

Figure 10. A portion of the previous image, from 0 to 400 s.

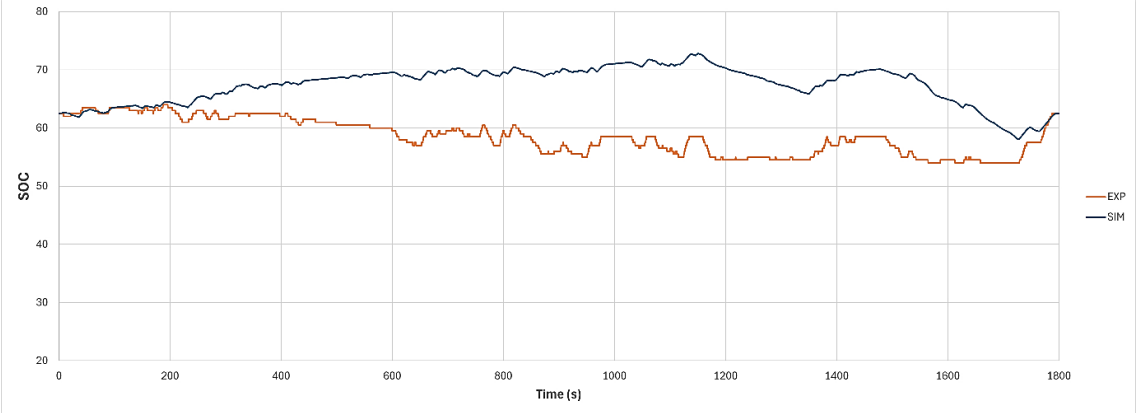

Figure 11. State of charge during the WLTP cycle with the EMS proposed in this study.

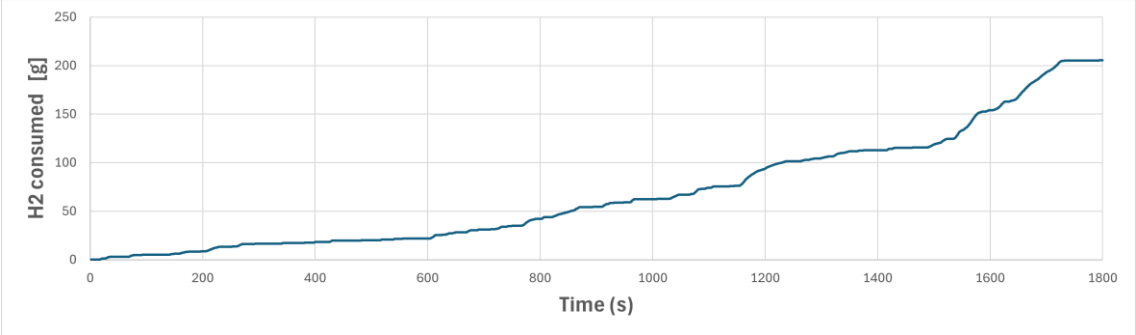

Figure 12. Hydrogen consumed to perform a WLTP cycle.

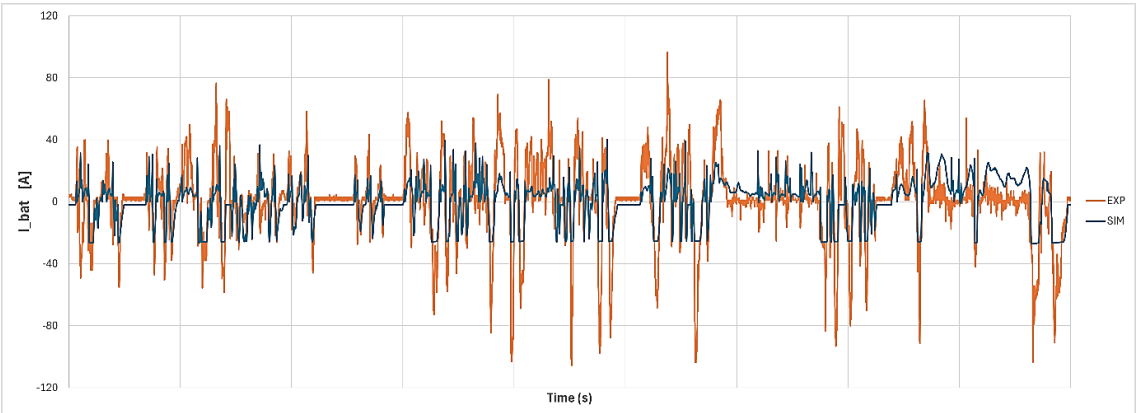

Figure 13. Differences between the current supplied by the battery during the simulation and in the real case.

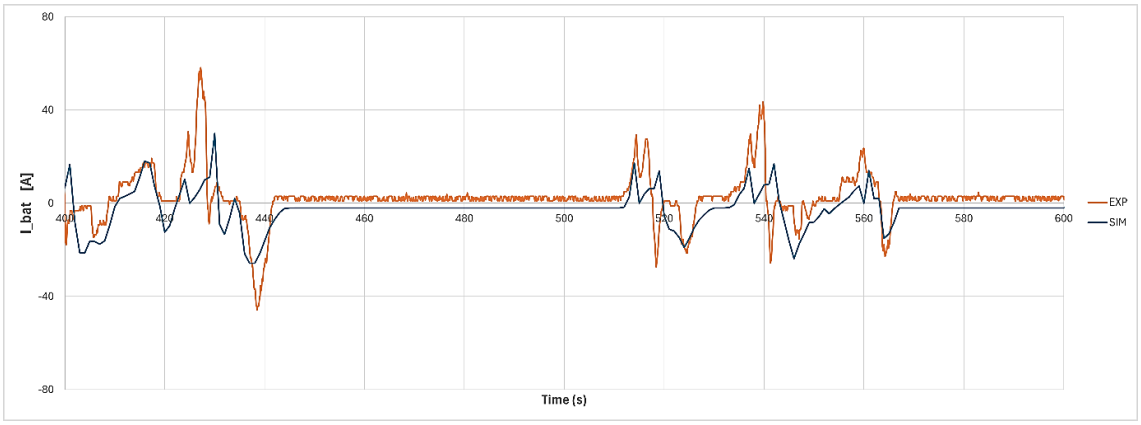

Figure 14. Enlarged section of the previous graph showing the linear trend of the current compared to the more complex system used in practice.

To keep the generality, the user can decide during the initialization if the graphs should be displayed in real time or if they should be displayed only at the end of the simulation. Some of the parameters that can be visualized are listed below. Figure 15 shows the monitor displaying the operating parameters during the simulation and, Figure 16 (left) shows the result of a simulation lasting 1000 WLTP cycles (corresponding to 500 hours), showing the drop in performance due to the aging of the stack, and Figure 16 (right) displays the percentage of power consumed by each auxiliary device.

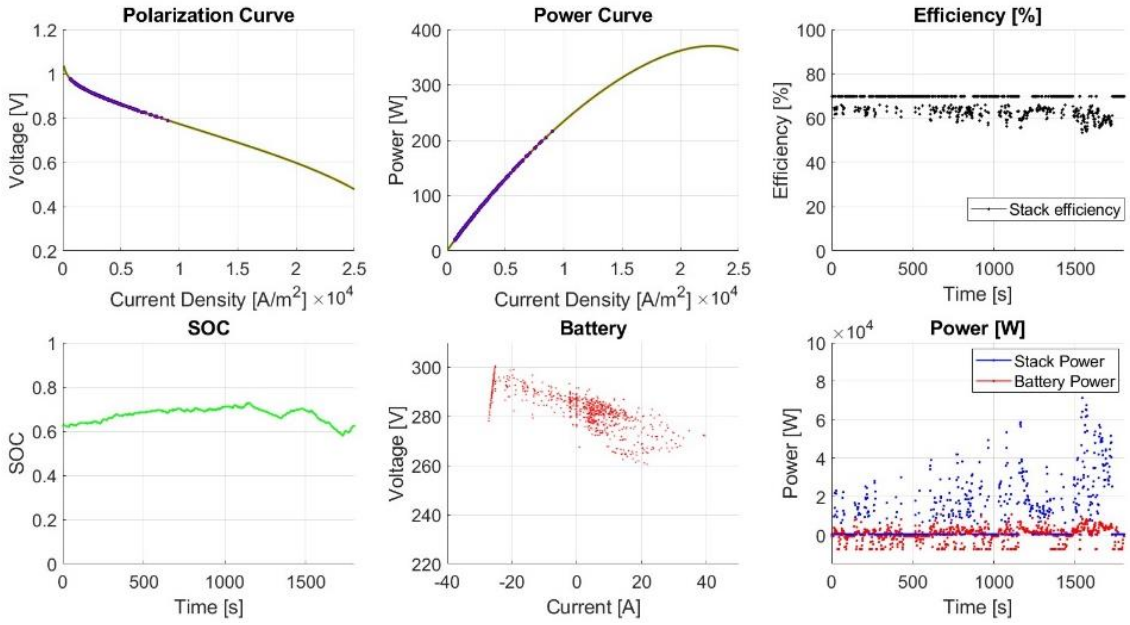

Figure 15. Run-time plots during a WLTP cycle.

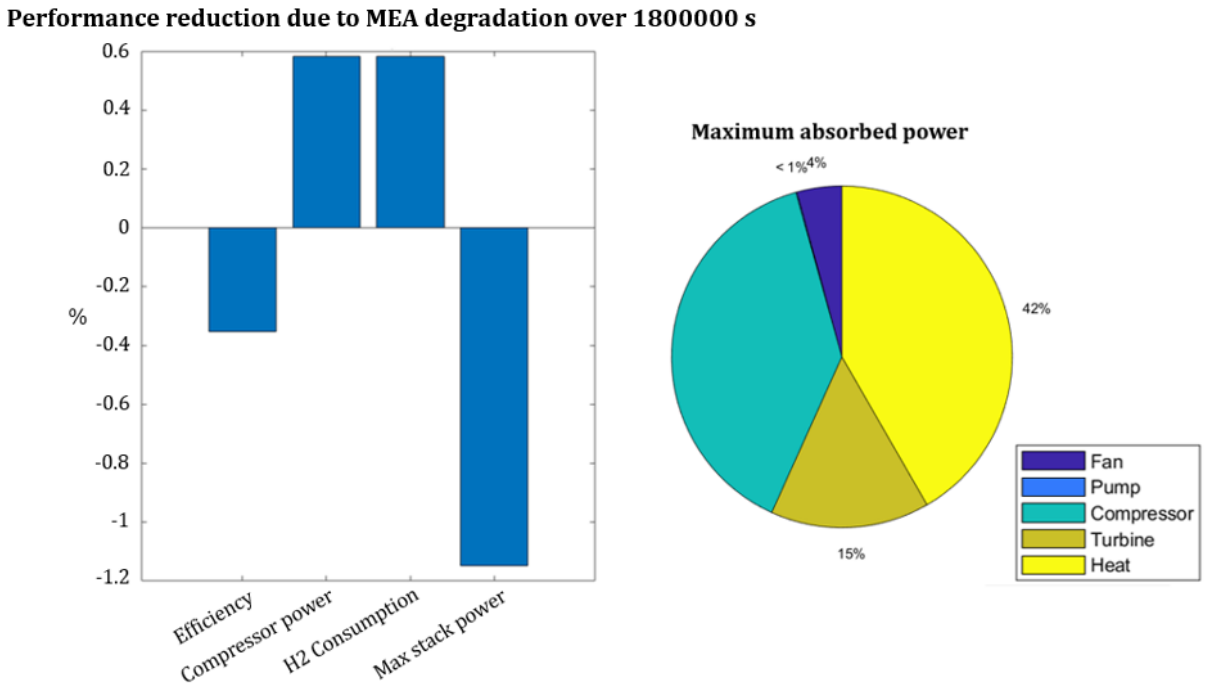

Figure 16. Drop in performance after 500 h of WLTP (left), and pie chart relative to the ancillaries' power demand (right).

5. Conclusions

This study has presented the development and analysis of a MATLAB/Simulink model for a hybrid battery/fuel cell vehicle (FCHEV). The model's performance has been evaluated against real-world data from the Toyota Mirai, provided by the Argonne National Laboratory. The comparison has shown a high agreement in terms of the tractive force required to move the vehicle. However, this validation has come with the caveat that the electric motor efficiency maps have not been available, which has introduced some error. It is important to note that since the implemented strategy has differed from the real-world strategy, other observed parameters have shown a different, more linear behaviour; this deviation has underscored the impact of control strategies on vehicle performance metrics. Nevertheless, the correlation in tractive force has suggested that the model is reliable for simulating the mechanical aspects of the hybrid powertrain.

Implementing the control strategy with Stateflow has ensured that the battery maintains a minimum state of charge (SOC). This is crucial for the vehicle to cope with different driving scenarios, from short city trips to long highway journeys, in accordance with the Worldwide Harmonized Light Vehicles Test Procedure (WLTP). The ability to adapt to different driving conditions without draining the battery has enhanced the model versatility and scalability.

The model's rule-based strategy has resulted in a 4.18% increase in fuel consumption. However, this trade-off has been offset by the significantly lower and more stable current drawn from the battery. The reduced and linear battery discharge profile has indicated a reduced load on the battery, potentially extending its life and ensuring more consistent performance.

The developed graphical user interface (GUI) has enhanced the usability of the model, making it a versatile tool for both academic research and next-generation powertrain development. The GUI has allowed users to easily experiment with different scenarios and control strategies, facilitating a deeper understanding of hybrid powertrain dynamics and optimization.

Research and development of hybrid battery/fuel cell powertrains is essential for the future of sustainable transportation. This technology offers a viable alternative to battery-only electric vehicles and contributes to the fight against climate change. By leveraging the strengths of both battery and fuel cell systems, hybrid vehicles can achieve zero emissions and improved efficiency, in line with the efforts to reduce the global warming. Moreover, this study has highlighted the significant role of zero-dimensional models in understanding the behaviour of complex systems, specifically in the context of hybrid powertrains for passenger cars.

6. Appendix

In this paper, the following acronyms are used:

- CNR-STEMS: National Research Council - Institute of Sciences and Technologies for Sustainable Energy and Mobility
- PEMFC: Proton Exchange Membrane Fuel Cell
- FC: Fuel Cell
- FCHEV: Fuel Cell Hybrid Electric Vehicle
- GUI: Graphic User Interface
- BoP: Balance of Plant
- SOC: State Of Charge
- EM: Electric Motor
- WLTP: Worldwide Harmonized Light Vehicles Test Procedure
- WMTC: Worldwide Motorcycle Test Cycle
- NEDC: New European Driving Cycle
- SFUDS: Supplemental Federal Test Procedure
- EMS: Energy Management System
- ESS: Energy Storage System
- NiMH: Nickel-Metal-Hydride battery pack
- OCV: Open Circuit Voltage
- H2: Hydrogen

Acknowledgement

The authors gratefully acknowledge the partial financial support of the European Union, NextGenerationEU - in the framework of the National Sustainable Mobility Center - MOST, CN00000023, Italian Ministry of University and Research Decree n. 1033 - 17/06/2022, Spoke 12, CUP B43C22000440001 (CNR STEMS) and CUP E93C22001070001 (University of Modena and Reggio Emilia).

References

[1] R. Lin, F. Xiong, W. C. Tang, L. Técher, J. M. Zhang, and J. X. Ma, “Investigation of dynamic driving cycle effect on the degradation of proton exchange membrane fuel cell by segmented cell technology,” *J Power Sources*, vol. 260, pp. 150–158, Aug. 2014, doi: 10.1016/J.JPOWSOUR.2014.03.003.

[2] A. Kerviel *et al.*, “An Evaluation of Turbocharging and Supercharging Options for High-Efficiency Fuel Cell Electric Vehicles,” *Applied Sciences 2018, Vol. 8, Page 2474*, vol. 8, no. 12, p. 2474, Dec. 2018, doi: 10.3390/APP8122474.

[3] M. P. Bakht, Z. Salam, A. R. Bhatti, W. Anjum, S. A. Khalid, and N. Khan, "Stateflow-Based Energy Management Strategy for Hybrid Energy System to Mitigate Load Shedding," *Applied Sciences 2021, Vol. 11, Page 4601*, vol. 11, no. 10, p. 4601, May 2021, doi: 10.3390/APP11104601.

[4] O. Tremblay and L. A. Dessaint, "Experimental Validation of a Battery Dynamic Model for EV Applications," *World Electric Vehicle Journal 2009, Vol. 3, Pages 289-298*, vol. 3, no. 2, pp. 289–298, Jun. 2009, doi: 10.3390/WEVJ3020289.

[5] G. Corda, S. Breda, A. D'Adamo, G. Corda, S. Breda, and A. D'Adamo, "A MATLAB/Simulink Model of a PEM Fuel Cell System Including Ageing Phenomenon," *SAE Technical Papers*, Aug. 2023, doi: 10.4271/2023-24-0148.

[6] A. D'Adamo, M. Haslinger, G. Corda, J. Höflinger, S. Fontanesi, and T. Lauer, "Modelling Methods and Validation Techniques for CFD Simulations of PEM Fuel Cells," *Processes 2021, Vol. 9, Page 688*, vol. 9, no. 4, p. 688, Apr. 2021, doi: 10.3390/PR9040688.

[7] A. D'Adamo, M. Riccardi, C. Locci, M. Romagnoli, and S. Fontanesi, "Numerical Simulation of a High Current Density PEM Fuel Cell," *SAE Technical Papers*, no. 2020, Sep. 2020, doi: 10.4271/2020-24-0016.

[8] A. D'Adamo, M. Riccardi, M. Borghi, and S. Fontanesi, "CFD Modelling of a Hydrogen/Air PEM Fuel Cell with a Serpentine Gas Distributor," *Processes 2021, Vol. 9, Page 564*, vol. 9, no. 3, p. 564, Mar. 2021, doi: 10.3390/PR9030564.

[9] G. Corda, S. Fontanesi, and A. d'Adamo, "Methodology for PEMFC CFD Simulation Including the Effect of Porous Parts Compression," *Int J Hydrogen Energy*, Mar. 2022, doi: 10.1016/J.IJHYDENE.2022.02.201.

[10] James. Larminie and J. Lowry, "Electric vehicle technology explained," p. 342, 2012, Accessed: Sep. 30, 2022. [Online]. Available: https://www.wiley.com/en-us/Electric+Vehicle+Technology+Explained%2C+2nd+Edition-p-9781119942733

[11] M. Carignano and R. Costa-Castello, "Toyota Mirai: Powertrain Model and Assessment of the Energy Management," *IEEE Trans Veh Technol*, Jun. 2023, doi: 10.1109/TVT.2023.3237173.

[12] M. Carignano, V. Roda, R. Costa-Castelló, L. Valiño, A. Lozano, and F. Barreras, "Assessment of Energy Management in a Fuel Cell/Battery Hybrid Vehicle", doi: 10.1109/ACCESS.2018.2889738.

[13] U. Usmanov, S. Ruzimov, A. Tonoli, and A. Mukhitdinov, "Modeling, Simulation and Control Strategy Optimization of Fuel Cell Hybrid Electric Vehicle," *Vehicles 2023, Vol. 5, Pages 464-481*, vol. 5, no. 2, pp. 464–481, Apr. 2023, doi: 10.3390/VEHICLES5020026.

[14] H. Lohse-Busch, K. Stutenberg, M. Duoba, and S. Iliev, "Technology Assessment Of A Fuel Cell Vehicle: 2017 Toyota Mirai," Jan. 2018, doi: 10.2172/1463251.

[15] L. Karpenko-Jereb, C. Sternig, C. Fink, and R. Tatschl, "Membrane degradation model for 3D CFD analysis of fuel cell performance as a function of time," *Int J Hydrogen Energy*, vol. 41, no. 31, pp. 13644–13656, Aug. 2016, doi: 10.1016/J.IJHYDENE.2016.05.229.